Inorg. Chem. **2002**, *41*, 2368–2373

Thermodynamic and Kinetic Control over the Reduction Mechanism of the $Pd_3(dppm)_3(CO)(I)^+$ Cluster

Frédéric Lemaître,[1a,b] David Brevet,[1a] Dominique Lucas,[1a] Alain Vallat,[1a] Yves Mugnier,*[,1a] and Pierre D. Harvey*[,1b]

Laboratoire de Synthèse et d'Electrosynthèse Organométalliques, CNRS UMR 5632, Faculté des Sciences Gabriel, Université de Bourgogne, 6 Boulevard Gabriel, 21000 Dijon, France, and Département de Chimie, Université de Sherbrooke, Sherbrooke, Québec, Canada J1K 2R1

Received July 10, 2001

The reduction mechanism of the title cluster has been investigated by means of cyclic voltammetry (CV), rotating disk electrode (RDE) voltammetry, and coulometry. The 2-electron reduction proceeds via two routes simultaneously. The first one involves two 1-electron reduction steps, followed by an iodide elimination to form the neutral $Pd_3(dppm)_3(CO)^0$ cluster (EEC mechanism). The second one is a 1-electron reduction process, followed by an iodide elimination, then by a second 1-electron step (ECE mechanism) to generate the same final product. Control over these two competitive mechanisms can be achieved by changing temperature, solvent polarity, iodide concentration, or sweep rate. The reoxidation of the $Pd_3(dppm)_3(CO)^0$ cluster in the presence of iodide proceeds via a pure ECE pathway. The overall results were interpreted with a six-member square scheme, and the cyclic and RDE voltammograms were simulated, in order to extract the reaction rate and equilibrium constants for iodide exchange for all three $Pd_3(dppm)_3(CO)(I)^n$ ($n = +1, 0, -1$) adducts.

Introduction

Since the first report on the synthesis and characterization of the $Pd_3(dppm)_3(CO)^{2+}$ cluster (dppm = bis(diphenylphosphino)methane) in the 1980s, by Puddephatt et al.,[2,3] and its Pt analogue,[4] numerous and exhaustive works on its reactivity and properties have appeared in the literature.[5−7] This cluster exhibits a triangular Pd_3 frame with three dppm-supported M−M single bonds. While one M_3 face is capped by a CO group, the other one is unsaturated, giving rise to rich coordination chemistry.[5−8] The dppm-phenyl groups form a cavity above this M_3 plane, limiting access to smaller substrates only.[6,7] Of particular interest in this work, the binding of halide ions onto this Pd_3^{2+} species leads to very stable architectures,[8,9] and the approximated binding constants spectroscopically evaluated by UV−visible methods indicate that the stability varies as I ≫ Br ≫ Cl.[10−12]

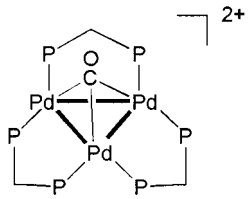

1

The reduction electrochemical properties of $Pd_3(dppm)_3(CO)^{2+}$ (**1**) were recently reported by our groups for both the PF_6^- (**1a**) and $CF_3CO_2^-$ (**1b**) salts.[13] This cationic cluster exhibits a 2-electron-reduction process, and depending upon the counteranion or the solvent, this event can appear either as a single 2-electron step or two 1-electron peaks on the cyclic voltammogram. The 2-electron transfer reaction, which can be discriminated into its 1-electron individual steps, has been the topic of many studies.[14] In a more general sense, the chemical processes which cause such phenomena are numerous and may involve, for example, isomerization, dimerization, and protonation reactions.

* To whom correspondence should be addressed. P.D.H.: tel, (819) 821-8000 ext. 2005; fax, (819) 821-8017; E-mail, pharvey@courrier.usherb.ca. Y.M.: tel and fax, (33) 3 80 39 60 91; E-mail, Yves.Mugnier@u-bourgogne.fr.

(1) (a) Université de Bourgogne. (b) Université de Sherbrooke.
(2) Manojlovic-Muir, L. J.; Muir K. W.; Lloyd, B. R.; Puddephatt, R. J. *J. Chem. Soc., Chem. Commun.* **1983**, 1336.
(3) Lloyd, B. R.; Puddephatt, R. J. *Inorg. Chim. Acta* **1984**, *90*, L77.
(4) Ferguson, G.; Lloyd, B. R.; Puddephatt, R. J. *Organometallics* **1986**, *5*, 344−348.
(5) Review article was published on the topic, see: Puddephatt, R. J.; Manojlovic-Muir, L.; Muir, K. W. *Polyhedron* **1990**, *9*, 2767 and the references therein.
(6) Harvey, P. D.; Crozet, M.; Aye, K. T. *Can. J. Chem.* **1995**, *73*, 123.
(7) Harvey, P. D.; Hubig, S.; Ziegler, T. *Inorg. Chem.* **1994**, *33*, 3700.
(8) Manojlovic-Muir, L.; Muir K. W.; Lloyd, B. R.; Puddephatt, R. J. *J. Chem. Soc., Chem. Commun.* **1985**, 536.

10.1021/ic0107328 CCC: $22.00
Published on Web 03/30/2002

Recently we also reported the electrochemically induced R−Br and R−I bond cleavage by the generated paramagnetic $Pd_3(dppm)_3(CO)^+$ intermediate cluster via a pathway producing "R^+" and "X^-".[15] One of the driving forces of this reactivity is the great affinity of the unsaturated Pd_3^{2+} center toward Br^- and I^-, leading to the final inorganic products $Pd_3(dppm)_3(CO)(X)^+$ ($X = Br^-$, I^-). The corresponding neutral $Pd_3(dppm)_3(CO)(X)^0$ proposed intermediates proved to be stable at the time scale of electrochemistry.

With respect to these findings, we now wish to report the electroreduction properties of **1** and its I^- adduct using CV, RDE voltammetry, and coulometry. Emphasis is placed upon the iodo derivative in this work, since it exhibits a complex electrochemical behavior with well-defined waves. The results are analyzed using a six-member square scheme, where the mechanism may vary according to iodide concentration, temperature, and sweep scans. Curve simulations of the voltammetric results enable us to extract both kinetic and thermodynamic data, such as binding constants, which are found to vary with the Pd oxidation state. The mechanism is also found to be dependent upon the halide (Cl^-, Br^-, I^-) and the solvent.

Experimental Section

Materials. The $[Pd_3(dppm)_3(CO)](PF_6)_2$ complex (**1a**) has been prepared according to literature procedures.[2,3] NBu_4I was purchased from Fluka and used as received. Tetrahydrofuran (THF) was distilled under Ar over Na and benzophenone, and acetonitrile over CaH_2. The supporting electrolyte used in each experiment was NBu_4PF_6 (Aldrich). The salt was recrystallized twice in ethanol and dried at 80 °C for at least 2 days before use.

Electrochemical Experiments. All manipulations were performed using Schlenk techniques in an atmosphere of dry oxygen-free argon gas. The supporting electrolyte was degassed under vacuum before use and then solubilized at a concentration of 0.2 M. For cyclic voltammetry experiments, the concentration of the analyte was nearly 10^{-3} M. Voltammetric analyses were carried out in a standard three-electrode cell with a Tacussel UAP4 unit cell. The reference electrode was a saturated calomel electrode (SCE) separated from the solution by a sintered glass disk. The auxiliary electrode was a platinum wire. For all voltammetric measurements, the working electrode was a vitreous carbon electrode ($\phi = 3$ mm) except for the experiment at high sweep rate where a semi-microelectrode of platinum ($\phi = 125$ μm) was used. In these conditions, when operating in THF, the formal potential for the ferrocene$^{+/-}$ couple is found to be +0.56 V versus SCE. The controlled potential electrolysis was performed with an Amel 552 potentiostat coupled with an Amel 721 electronic integrator. High-scale electrolyses were performed in a cell with three compartments separated with fritted glasses of medium porosity. A carbon gauze was used as the working electrode, a platinum plate as the counter electrode, and a saturated calomel electrode as the reference electrode.

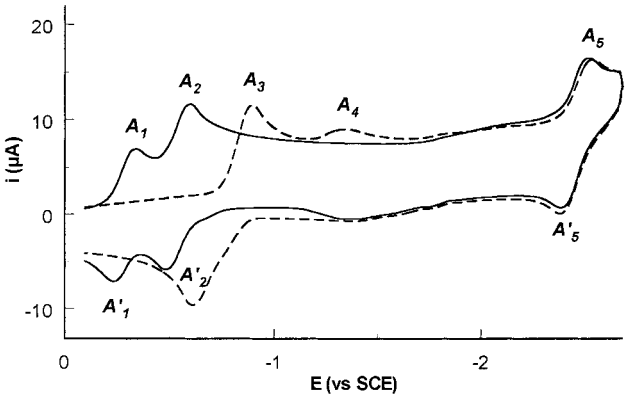

Figure 1. Cyclic voltammogram of 0.68 mM $[Pd_3(dppm)_3(CO)](PF_6)_2$, **1a**, in THF: (a, solid line) **1a** alone; (b, dashed line) after addition of 1.1 molar equiv of NBu_4I. Initial potential: −0.1 V. Scan rate: 100 mV·s^{-1}.

Digital Simulation. The computations were performed using the commercially available program called Digisim (Bioanalytical systems). The potential increase was set to 5 mV. The uncompensated resistance, here $R_u = 1500$ Ω, was determined with a PAR 373A potentiostat using the same experimental conditions as for the CV measurements. The double-layer capacitance value was estimated as $C_{dl}/A = 10^{-4}$ F·cm^{-2} using a blank solution prior to voltammetric measurements. The experimental curves were corrected for residual current, also determined using voltammetric measurements of blank solutions.

Results and Discussion

Reduction of 1 and $Pd_3(dppm)_3(CO)(I)^+$: Mechanism Overview. Figure 1 (curve a) shows the cyclic voltammogram of **1a** (PF_6^- salt) in THF containing 0.2 M NBu_4PF_6, which exhibits two electrochemically reversible systems at $E_{1/2} = -0.29$ V (peaks A_1 and A'_1) and −0.54 V (peaks A_2 and A'_2) vs SCE.[16] These peaks correspond to the following redox processes:

$$\underset{\mathbf{1}}{Pd_3(dppm)_3(CO)^{2+}} + e^- \rightleftharpoons Pd_3(dppm)_3(CO)^+ \qquad (1)$$

$$Pd_3(dppm)_3(CO)^+ + e^- \rightleftharpoons Pd_3(dppm)_3(CO)^0 \qquad (2)$$

Coulometric measurements indicate that these processes are 1-electron.[13] The neutral species $Pd_3(dppm)_3(CO)^0$ can also be generated electrochemically from $Pd(dppm)Cl_2$ and

(9) (a) The triangular structure "$M_3(dppm)_3(\mu\text{-}X)(\mu\text{-}Y)^{n+}$" (X = halide; Y = halide or donor) is very common for low-valent late transition metals such as Ni, Pd, Pt, Cu, and Ag. See for examples:[9b−j] (b) Balch, A. L.; Davis, B. J.; Olmstead, M. M. *Inorg. Chem.* **1993**, *32*, 3937. (c) Balch, A. L.; Davis, B. J.; Olmstead, M. M. *J. Am. Chem. Soc.* **1990**, *112*, 8592. (d) Douglas, G.; Jennings, M. C.; Manojlovic-Muir, L.; Puddephatt, R. J. *Inorg. Chem.* **1988**, *27*, 4516. (e) Ratliff, K. S.; Fanwick, P. E.; Kubiak, C. P. *Polyhedron* **1990**, *9*, 1487. (f) Morgenstern, D. A.; Ferrence, G. M.; Washington, J.; Henderson, J. I.; Rosenhein, L.; Heise, J. D.; Fanwick, P. E.; Kubiak, C. P. *J. Am. Chem. Soc.* **1996**, *118*, 2198. (g) Morgenstern, D. A.; Wittrig, R. E.; Fanwick, P. E.; Kubiak, C. P. *J. Am. Chem. Soc.* **1993**, *115*, 6470. (h) Camus, A.; Marsich, N.; Nardin, G.; Randaccio, L. *J. Organomet. Chem.* **1973**, *60*, C39. (i) Aly, A. A. M.; Neugebauer, D.; Orama, O.; Schubert, U.; Schmidbauer, H. *Angew. Chem., Int. Ed. Engl.* **1978**, *17*, 125. (j) Schubert, U.; Neugebauer, D.; Aly, A. A. M. *Z. Anorg. Allg. Chem.* **1980**, *464*, 217.

(10) Harvey, P. D.; Provencher, R.; Gagnon, J.; Zhang, T.; Fortin, D.; Hierso, K.; Drouin, M.; Socol, S. M. *Can. J. Chem.* **1996**, *74*, 2268.

(11) Zhang, T.; Drouin, M.; Harvey, P. D. *Chem. Commun.* **1996**, 877.

(12) Harvey, P. D.; Hierso, K.; Braunstein, P.; Morise, X. *Inorg. Chim. Acta* **1996**, *250*, 337.

(13) Gauthron, I.; Mugnier, Y.; Hierso, K.; Harvey, P. D. *Can. J. Chem.* **1997**, *75*, 1182.

(14) Pierce, D. T.; Geiger, W. E. *J. Am. Chem. Soc.* **1992**, *114*, 6063 and refs 28−43 therein.

(15) Brevet, D.; Lucas, D.; Cattey, H.; Lemaître, F.; Mugnier, Y.; Harvey, P. D. *J. Am. Chem. Soc.* **2001**, *123*, 4340.

(16) $E_{1/2}$ is defined as $^1/_2(E_{p,a} + E_{p,c})$.

Scheme 1

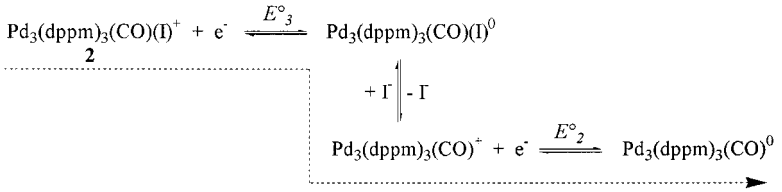

ECE reduction pathway for **2** *leading to the 2-electron peak* A_3 ($E°_2 > E°_3$)

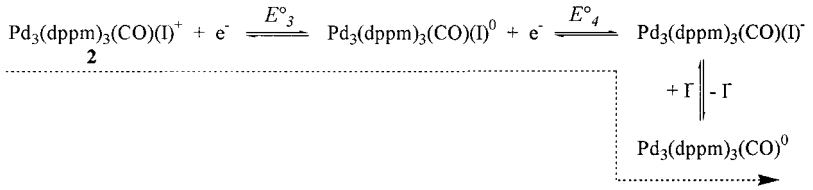

EEC reduction pathway for **2** *leading to the two 1-electron peaks* A_3 *and* A_4 ($E°_4 < E°_3$)

$Pd_2(dppm)_2Cl_2$ in the presence of CO_2 in aprotic media, suggesting that the Pd_3 frame appears relatively stable, at least, under inert atmosphere for this oxidation state.[17]

In addition, a new reversible reduction system (peaks A_5 and A'_5) is depicted at a significantly more negative potential ($E_{1/2} = -2.45$ V vs SCE), and on the basis of the relative peak current, this process is assigned to a 1-electron reduction as described below:

$$Pd_3(dppm)_3(CO)^0 + e^- \rightleftharpoons Pd_3(dppm)_3(CO)^- \qquad (3)$$

Upon addition of iodide (1.1 molar equiv of NBu_4I), the cyclic voltammogram undergoes drastic changes (Figure 1; curve b), which predictably indicate the formation of the corresponding adduct $Pd_3(dppm)_3(CO)(I)^+$ (**2**). This identification is confidently confirmed with the comparison with an authentic sample.[8] From ^{31}P NMR spectroscopy, this reaction is found complete where the signal associated with the starting material **1a** ($\delta = -1.3$ ppm) is converted into **2** ($\delta = -6.4$ ppm) upon addition of the iodide salt. In cyclic voltammetry, the new reduction processes occur at -0.89 V (peak A_3 at 100 mV/s) and at -1.34 V vs SCE (peak A_4 at 100 mV/s), noticeably not with the same current magnitude. The relative increase in the reduction potential for **2** (potential of peak A_3) compared to that of **1** (peak A_1) appears consistent with an increase in electron density at the Pd_3 center due to iodide coordination. The peak system, at more negative potential (peaks A_5 and A'_5), remains practically unchanged at -2.45 V vs SCE. This result indicates that the presence of iodide salt does not influence reaction 3, either at all or not significantly. In conclusion, the 2-electron reduction of **2** leads to the complete elimination of iodide as defined by eq 4.

$$\underset{\mathbf{2}}{Pd_3(dppm)_3(CO)(I)^+} + 2e^- \rightleftharpoons Pd_3(dppm)_3(CO)^0 + I^- \quad (4)$$

As anticipated, coulometric measurements on a carbon gauze electrode at an applied potential of -0.9 V vs SCE indicate that 2 F/mol ($n_{exp} = 2.06$ F/mol) are consumed during the bulk electrolysis of **2**. The cyclic voltammogram of the resulting solution exhibits the expected reduction peak A_5, demonstrating that $Pd_3(dppm)_3(CO)^0$ is the species formed in the bulk of the solution.

The following section addresses the mechanism of this electrochemical reaction which can be formalized according to Scheme 1. Two pathways are possible, which are defined as ECE and EEC with E and C being electrochemical electron transfer and chemical halide exchange events, respectively.

An EEC mechanism implies that two 1-electron peaks should be observed as the $Pd_3(dppm)_3(CO)(I)^+$ species should be easier to reduce than the neutral $Pd_3(dppm)_3(CO)(I)^0$ cluster. On the other hand, the reduction of $Pd_3(dppm)_3(CO)^+$ in $Pd_3(dppm)_3(CO)^0$ (eq 2) being at lower negative potential than that of $Pd_3(dppm)_3(CO)(I)^+$ in $Pd_3(dppm)_3(CO)(I)^0$ (peak A_3 only at -0.895 V) indicates that the ECE pathway should lead to a single 2-electron peak. Experimentally, two peaks of different current magnitudes are observed (see Figure 1; curve b), which indicates that in fact both mechanisms are present. The weaker peak A_4 witnesses the presence of an EEC mechanism. In principle the EEC mechanism leads to two reduction peaks of similar current magnitude. Experimentally peak A_3 exhibits a greater height, which indicates that the competitive ECE pathway is also effective simultaneously. This double mechanism is well illustrated in Figure 2 (curve a) in the RDE voltammogram of **2**, where waves A_3 and A_4 are evident. On the basis of their heights, it is possible to quantify the relative contribution of the ECE and EEC pathways. In this case, the EEC pathway contributes to about 80% of the 2-electron reduction of **2** ($\% = 2i_{d,A_4}/(i_{d,A_3} + i_{d,A_4}) \times 100$) where i_{d,A_3} and i_{d,A_4} are the heights of waves A_3 and A_4, respectively), leaving 20% for the ECE pathway.

(17) Gauthron, I.; Mugnier, Y.; Hierso, K.; Harvey, P. D. *New J. Chem.* **1998**, 247.

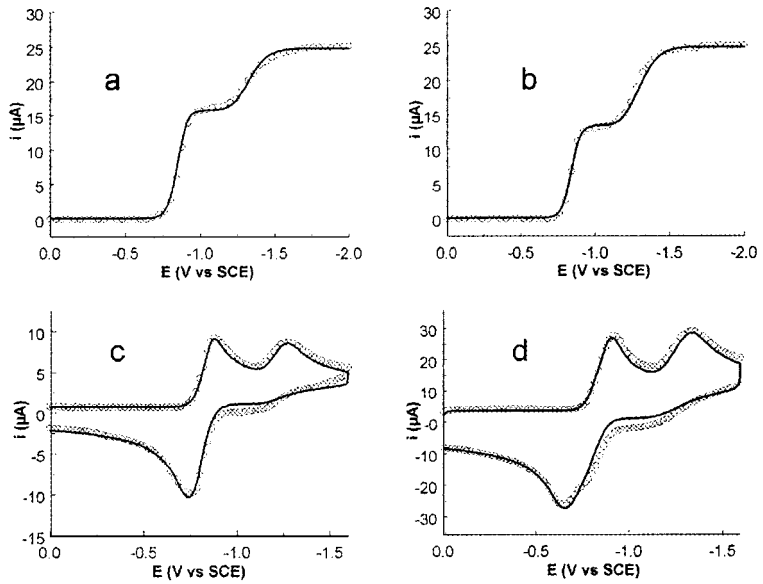

Figure 2. Digital simulations (solid line) compared to experimental (circles) RDE and CV scans. Experimental conditions: solvent, THF; [**2**] = 0.78 mM (a, b) and 1.12 mM (c, d); $[I^-]$ = 0 mM (a), 7.02 mM (b), and 10.08 mM (c, d); scan rate, 20 mV·s^{-1} (a, b), 50 mV·s^{-1} (c), and 500 mV·s^{-1} (d).

Scheme 2

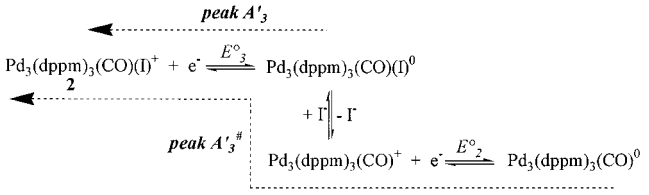

The reduction of **2** (eq 4) is found to be chemically reversible. Indeed, coulometric measurement for the $Pd_3(dppm)_3(CO)^0$ product arising from the electrolysis of **2** (see above) indicates that complete reoxidation also requires 2 F/mol (n_{exp} = 2.05 F/mol), and the cyclic voltammogram is identical to that of curve b in Figure 1. The overall reoxidation process can be written as

$$Pd_3(dppm)_3(CO)^0 + I^- - 2e^- \rightleftharpoons Pd_3(dppm)_3(CO)(I)^+ \quad (5)$$

A close examination of the return peaks for **2** in THF with 0.2 M NBu_4PF_6 reveals a peak $A'_3{}^{\#}$ at −0.62 V and a shoulder A'_3 at ∼−0.75 V vs SCE (see Figure 3; curve a), each corresponding, respectively, to the oxidation of $Pd_3(dppm)_3(CO)^0$ and $Pd_3(dppm)_3(CO)(I)^0$ species which, as they have been observed, in the reductive scan, also appear in the oxidative scan. It must be noted that peak $A'_3{}^{\#}$ (E_p = −0.62 V) is far from the same peak observed in the absence of free iodide (peak A'_2 on Figure 1a, E_p = −0.41 V), which is the diagnostic of a univocal oxidation pathway (see Scheme 2) where the kinetics of the intermediate chemical reaction cause a shift in the potential of the peak associated with the first electrochemical step.[18] This observation is corroborated with the CV curve simulation described below, which shows that the EEC mechanism does not participate at all in the oxidation of $Pd_3(dppm)_3(CO)^0$. The CEE pathway itself can be excluded since peak A_4 is found irreversible.

(18) Noel, M.; Vasu, K. I. *Cyclic Voltammetry and the Frontiers of Electrochemistry*; Aspect Publications Ltd.: London, 1990.

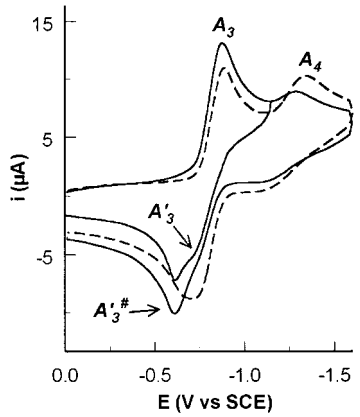

Figure 3. Cyclic voltammogram of 0.83 mM $[Pd_3(dppm)_3(CO)(I)](PF_6)$, **2**, in THF: (a, solid line) **2** alone; (b, dashed line) after addition of 9 molar equiv of NBu_4I. Initial potential: 0 V. Scan rate: 100 mV·s^{-1}.

Figure 3a shows that the relative height of $A'_3{}^{\#}$ depends on whether the potentiel scan is inverted after reduction peak A_4 or A_3. When inverting after A_4, $A'_3{}^{\#}$ is significantly larger. Indeed, at the potential of A_4, the conversion of $Pd_3(dppm)_3(CO)(I)^+$ in $Pd_3(dppm)_3(CO)^0$ is completed, resulting in an increase of the relative amount of $Pd_3(dppm)_3(CO)^0$ at the electrode. However, peak A'_3 is still appearing due to continuous diffusion of $Pd_3(dppm)_3(CO)(I)^+$ from the bulk of the solution to the electrode. In contrast, the same voltammetric scan, recorded under identical conditions but with $Pd_3(dppm)_3(CO)^0$ in solution (e.g., after electrolysis of $Pd_3(dppm)_3(CO)(I)^+$ at −0.9 V vs SCE, as described above), does not provide peak A'_3, but peak $A'_3{}^{\#}$ alone (figure available in Supporting Information).

Change in Iodide Concentration. Addition of 9 equiv of NBu_4I to **2** leads to an increase of peak A_4 and a decrease of peak A_3 (see Figure 3; curve b), indicating that the EEC reduction process is favored. These results are consistent with the increase at the electrode in $Pd_3(dppm)_3(CO)(I)^0$ concentration and a decrease in $Pd_3(dppm)_3(CO)^+$.

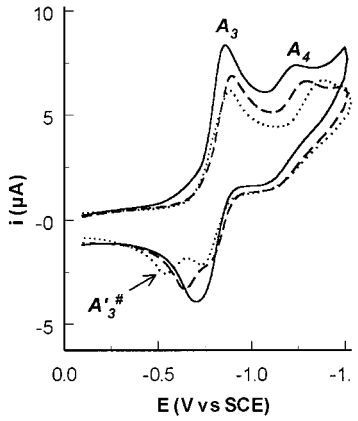

Figure 4. Cyclic voltammogram of 0.87 mM $[Pd_3(dppm)_3(CO)(I)](PF_6)$, **2**, in THF: (a, solid line) room temperature; (b, dashed line) $T = 0$ °C; (c, dotted line) $T = -10$ °C. Initial potential: −0.1 V. Scan rate: 100 mV·s^{-1}.

An examination of the RDE voltammogram of **2** in the presence of excess iodide (see Figure 2b) indicates that the heights of waves A_3 and A_4 are equal and do not change upon further addition of iodide. Under these experimental conditions, the EEC mechanism operates solely.

In CV, in the oxidative scan, as shown in Figure 3b, the return peaks A'_3 and $A'_3{}^{\#}$ appear as a single broad peak which exhibits a maximum at −0.74 V vs SCE, which is due to the shift of peak $A'_3{}^{\#}$ toward more negative potential as the recombination of I^- and $Pd_3(dppm)_3(CO)^+$ is rendered faster.

Effect of Sweep Rate. Similar changes in voltammetric curves are noted when sweep rate is varied. At high sweep rate, the EEC reduction pathway gains over the ECE one (relative increase of A_4 versus A_3 as observed from Figure 2c to 2d); the dissociation of $Pd_3(dppm)_3(CO)(I)^0$ becomes less effective due to the restricted duration of the scan. Regarding the oxidation part of the voltammogram, peaks A'_3 and $A'_3{}^{\#}$ appear better separated at high sweep rate as $A'_3{}^{\#}$ is expected to move toward a more positive potential.[18]

With 50−500 mV/s sweep rates, peak A_4 appears to be irreversible, indicating that $Pd_3(dppm)_3(CO)(I)^-$ is extremely unstable. Using a semi-microelectrode with a scan rate of 100 V/s, the oxidation peak for this species can be observed at $E_p = -1.24$ V vs SCE, which indicates a relative lifetime on the millisecond time scale.

Lowering the Temperature. Temperature provides direct control over the kinetics of the dissociation of $Pd_3(dppm)_3(CO)(I)^0$ as well as its re-formation. Lowering the temperature to −10 °C results in a nearly exclusive EEC reduction pathway where the heights of peaks A_3 and A_4 are in the same range (Figure 4, curve c). Similarly, from the reoxidation of $Pd_3(dppm)_3(CO)^0$, an evolution of the peak system $A'_3/A'_3{}^{\#}$ is obvious where at −10 °C both peaks are well separated, again due to the shift of $A'_3{}^{\#}$ to a more positive potential as one can predict when the reaction between $Pd_3(dppm)_3(CO)^+$ and I^- is slowed.[18]

Behavior of $Pd_3(dppm)_3(CO)(I)^+$ in Acetonitrile. The pathway can also be selected via an appropriate choice of the solvent. Based upon the known dissociation behavior of the iodide adducts, polar solvents should stabilize the dissociated ions. The use of acetonitrile instead of THF leads, at room temperature, to a cyclic voltammogram in which the reduction sweep exhibits only peak A_3 (see Supporting Information). This result indicates that only the ECE pathway is indeed effective, consistent with the strong tendency for $Pd_3(dppm)_3(CO)(I)^0$ to dissociate in the more polar solvent. The return sweep exhibits a single and broad peak at −0.73 V vs SCE assigned to the ECE oxidation mechanism.[19]

Behavior of the Chloride and Bromide Adducts. Cluster **1a** in the presence of an excess of Cl^- and Br^- (added as their tetrabutylammonium salts) generates the corresponding $Pd_3(dppm)_3(CO)(Cl)^+$ and $Pd_3(dppm)_3(CO)(Br)^+$ adducts as confirmed with authentic samples.[8] The cyclic voltammograms for both adducts exhibit a narrow single 2-electron-reduction peak at −0.81 and −0.87 V vs SCE (potential peak at 100 mV/s) for X = Cl^- and Br^-, respectively (CVs available in the Supporting Information). Similarly to $Pd_3(dppm)_3(CO)(I)^+$, the more negative potential for these species, with respect to **1**, is also consistent with an increase in electron density at the Pd_3 center. The key feature is that the corresponding A_4 peak is absent from the cyclic voltammogram, which indicates that the EEC reduction mechanism does not proceed in these cases. The reoxidation of the common $Pd_3(dppm)_3(CO)^0$ product also proceeds via a single 2-electron peak. No significant change in the shape of the voltammetric curves is observed when X^- concentration, sweep rate, or temperature is varied.

Simulations. The CV and RDE voltammograms of **2** have been simulated in relation with the 6-species square scheme[20] shown in Scheme 3. The best fits between experimental and theoretical curves (see Figure 2) were obtained with the parameters listed in Tables 1 and 2. The complete and detailed procedure can be found in the Supporting Information.

The simulation results provide both the equilibrium constants K_1, K_2, and K_3 and the iodide exchange rate constants k_{f2} and k_{f3} taken in the deshalogenation direction.[21] The fact that $K_1 < K_2 < K_3$ is consistent with the electrostatic properties of the cluster species. The small constant K_1 indicates that $Pd_3(dppm)_3(CO)(I)^+$ is essentially undissociated in THF.

Finally, we have found that the simulated curves were unchanged by suppressing $Pd_3(dppm)_3(CO)^{2+}$ and its reactions of the predefined mechanism in Digisim, which confirms that the EEC pathway does not participate at all in the oxidation of $Pd_3(dppm)_3(CO)^0$.

The bromide and chloride cyclic and RDE voltammograms were not simulated in this work. The voltammetric profiles are not sufficiently informative to allow any meaningful analysis.

(19) (a) This solvent dependence on the separation of two closely spaced redox waves into its two components has been observed for $Pd_3(dppm)_3(CO)^{2+}$,[13] and also for the closely related $Pd_4(dppm)_4(H)_2^{2+}$ species.[19b] (b) Gauthron, I.; Gagnon, J.; Zhang, T.; Rivard, D.; Lucas, D.; Mugnier, Y.; Harvey, P. D. *Inorg. Chem.* **1998**, *37*, 1112.

(20) Laviron, E. *J. Electroanal. Chem.* **1984**, *169*, 29.

(21) The comparison of the binding constants measured spectroscopically and electrochemically is expectedly poor because the solvent (methanol for UV−vis, and THF for electrochemistry) and the time scale of the experiments are different. The solvents are found to induce great changes in the equilibrium constants, if equilibrium exists.

Scheme 3

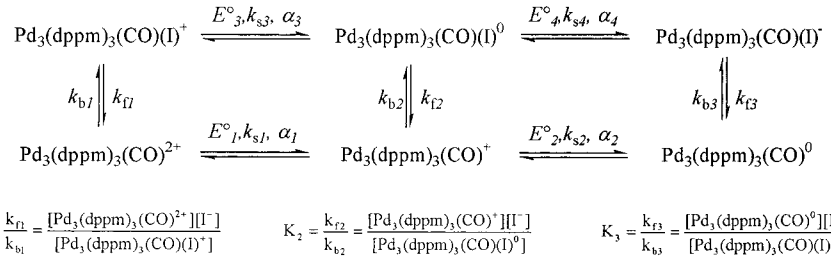

$$K_1 = \frac{k_{f1}}{k_{b1}} = \frac{[Pd_3(dppm)_3(CO)^{2+}][I^-]}{[Pd_3(dppm)_3(CO)(I)^+]} \qquad K_2 = \frac{k_{f2}}{k_{b2}} = \frac{[Pd_3(dppm)_3(CO)^+][I^-]}{[Pd_3(dppm)_3(CO)(I)^0]} \qquad K_3 = \frac{k_{f3}}{k_{b3}} = \frac{[Pd_3(dppm)_3(CO)^0][I^-]}{[Pd_3(dppm)_3(CO)(I)^-]}$$

Table 1. Input Data for Best Fits

$E°_i$ (V vs SCE)	k_{si} (cm·s^{-1})	α_i
$E°_1 = -0.295$	$k_{s1} \geq 0.2$	$\alpha_1 = 0.5$
$E°_2 = -0.54$	$k_{s2} \geq 0.2$	$\alpha_2 = 0.5$
$E°_3 = -0.83$	$k_{s3} \geq 0.2$	$\alpha_3 = 0.5$
$E°_4 = -1.28$	$k_{s4} = 0.005(3)$	$\alpha_4 = 0.5$

Table 2. Simulation Results

K_i (mol·L^{-1})	k_{fi} (s^{-1})
$K_1 = 3 \times 10^{-17}$ [a]	$k_{f1} = ?$[b]
$K_2 = 3.3 \times 10^{-8}$	$k_{f2} = 5 \times 10^{+3}$
$K_3 = 1.06 \times 10^{5}$	$k_{f3} = 500$

[a] Values smaller than 1×10^{-18} and greater than 1×10^{-16} mol·L^{-1} give unsatisfactory results. [b] This value can take a wide range of values and cannot be determined with confidence.

Concluding Remarks

This study shines more light on the mechanism for the recently reported electrochemically induced R−Br and R−I bond cleavage.[15] Indeed, this work establishes that **1** and $Pd_3(dppm)_3(CO)^+$ are very strong halide ion scavengers, potentially capable of binding any traces of these anions. For the R−Br and R−I molecules (R = alkyl groups), for which ionic dissociation is not favored, halides exist only at the concentration level of trace, still large enough to be detected by $Pd_3(dppm)_3(CO)^+$. The absence of direct reactivity between the stronger Lewis acid $Pd_3(dppm)_3(CO)^{2+}$ and alkyl halides is tentatively explained by the attraction between the Pd_3^{2+} center and counteranion (generally $CF_3CO_2^-$ or PF_6^-) which may considerably slow the halide trapping process.[22] Unpublished results demonstrate that $Pd_3(dppm)_3(CO)^{2+}$ reacts with R(CO)Cl to form $Pd_3(dppm)_3(CO)(Cl)^+$ and $R(CO)^+$ (trapped as $R(CO)(C_6H_4)(OCH_3)$ with anisole).[23]

The second observation is that halides added to the electrochemical solutions for the generation of the paramagnetic $Pd_3(dppm)_3(CO)^+$ species preclude subsequent C−Br and C−I activations. Indeed, the very small value for K_1 indicates that any trace of iodide is rapidly scavenged by the $Pd_3(dppm)_3(CO)^{2+}$ cluster forming the dead-end product $Pd_3(dppm)_3(CO)(I)^+$ in these C−X bond cleavage reactions. Experimentally, this poisoning by Cl^-, Br^-, and I^- is indeed observed.[15]

The small K_2 value (3.3×10^{-8} mol·L^{-1}) also indicates the strong tendancy of the paramagnetic cluster $Pd_3(dppm)_3(CO)^+$ to act as a very good iodide binder as well, and therefore the $Pd_3(dppm)_3(CO)(I)^0$ is stable. Experimentally, attempts to prepare this species from the direct reaction of $Pd_3(dppm)_3(CO)^+$ and I^- fail and lead to disproportionation according to reaction 6.

$$2Pd_3(dppm)_3(CO)^+ + I^- \rightleftharpoons Pd_3(dppm)_3(CO)(I)^+ + Pd_3(dppm)_3(CO)^0 \quad (6)$$

However, this reaction was found to be too slow to compete at the voltammetric time. Indeed, when included in the mechanism predefined in Digisim, it does not change the simulated results at all.

This study also demonstrates that iodide elimination from the Pd_3 cluster can be effective under reductive conditions. The greater K_3 value (1×10^5 mol·L^{-1}) implies that the $Pd_3(dppm)_3(CO)(I)^-$ cluster is entirely dissociated in $Pd_3(dppm)_3(CO)^0$ and I^-. Electrochemical regeneration of the $Pd_3(dppm)_3(CO)(I)^+$ cluster (reduction/I^- elimination/oxidation) provides hope for the design of catalytical systems for the synthesis of organic materials such as nonsymmetric ethers and esters via the use of the corresponding bromo and iodo derivatives. Investigations on these halide materials, acid halides and thiols, are in progress.

Acknowledgment. P.D.H. thanks NSERC (Natural Sciences and Engineering Research Council) and FCAR (Fonds Concertés pour l'Avancement de la Recherche) for funding. Y.M. is grateful to CNRS (Centre National de la Recherche Scientifique) and Conseil Régional de Bourgogne for funds. The authors thank also the referees for their helpful comments.

Supporting Information Available: Cyclic voltammograms of $[Pd_3(dppm)_3(CO)]^0$ in THF, of $Pd_3(dppm)_3(CO)(I)^+$ in acetonitrile, and of $Pd_3(dppm)_3(CO)(Br)^+$ and $Pd_3(dppm)_3(CO)(Cl)^+$ in THF and detailed procedure for the simulation of the voltammetric curves. This material is available free of charge via the Internet at http://pubs.acs.org.

IC0107328

(22) Very slow reactivity between **1** and a limited numbers of R−I substrates (R = CH_3, C_2H_5, *n*-C_4H_9, . . .) is observed. The same $Pd_3(dppm)_3(CO)(I)^+$ and R^+ products are found as in the electrochemically induced reactivity.[23]

(23) Lemaître, F.; Lucas, D.; Mugnier, Y.; Harvey, P. D. Unpublished results.